

Article

# The Surface Anodization of Titanium Dental Implants Improves Blood Clot Formation Followed by Osseointegration

Tonino Traini \* , Giovanna Murmura, Bruna Sinjari, Giorgio Perfetti, Antonio Scarano, Camillo D'Arcangelo and Sergio Caputi

Department of Medical, Oral and Biotechnological Sciences, University of Chieti-Pescara, Chieti 66100, Italy; g.murmura@unich.it (G.M.); b.sinjari@unich.it (B.S.); giorgio.perfetti@unich.it (G.P.); antonio.scarano@unich.it (A.S.); camillo.darcangelo@unich.it (C.D.); scaputi@unich.it (S.C.)

\* Correspondence: t.traini@unich.it; Tel.: +39-0871-3554143

Received: 2 June 2018; Accepted: 16 July 2018; Published: 20 July 2018



**Abstract:** The anodization of titanium dental implant influences the biologic processes of osseointegration. 34 grit-blasted and acid-etched titanium specimens were used to evaluate micro- and nano-roughness ( $R_a$ ), contact angle ( $\theta$ ) and blood clot extension ( $bce$ ). 17 samples were anodized (test) while the remaining were used as control. The  $bce$ , was measured using 10  $\mu$ L of human blood left in contact with titanium for 5 min at room temperature. The micro- and nano-scale  $R_a$  were measured under CLSM and AFM, respectively, while the  $\theta$  was analyzed using the sessile drop technique. The bone-implant contact ( $BIC$ ) rate was measured on two narrow implants retrieved for fracture.  $bce$  was 42.5 ( $\pm 22$ ) for test and 26.6% ( $\pm 13$ )% for control group ( $p = 0.049$ ). The micro- $R_a$  was 6.0 ( $\pm 1.5$ ) for the test and 5.8 ( $\pm 1.8$ )  $\mu$ m for control group ( $p > 0.05$ ). The  $\theta$  was 98.5° ( $\pm 18.7^\circ$ ) for test and 103° ( $\pm 15.2^\circ$ ) for control group ( $p > 0.05$ ). The nano- $R_a$  was 286 ( $\pm 40$ ) for the test and 226 ( $\pm 40$ ) nm for control group ( $p < 0.05$ ). The  $BIC$  rate was 52.5 ( $\pm 2.1$ ) for test and 34.5% ( $\pm 2.1$ )% for control implant ( $p = 0.014$ ). (Conclusions) The titanium anodized surface significantly increases blood clot retention, significantly increases nano-roughness, and favors osseointegration. When placing dental implants in poor bone quality sites or with immediate loading protocol anodized Ti6Al4V dental implants should be preferred.

**Keywords:** implant; topography; surface treatment; blood clot extension

## 1. Introduction

The contact between blood and titanium surface is the first phenomenon to occur during implant placement. It induces the fibrin clot formation, which plays a crucial role in implant osseointegration [1]. Since it has been reported that implants surface properties can modulate the extension of the above-mentioned fibrin network [2,3], they have to be considered among the factors that influence the early phase of osseointegration [4].

Several authors have evaluated the chemical and morphological features of implant surfaces [5–9] and their interaction with all blood components [10,11].

As soon as blood comes in contact with the titanium implant surface, the host plasma proteins are adsorbed on it [9,12]. As reported by Keselowsky [9], vitronectin, fibronectin and fibrinogen form a biofilm on the implant surface which acts as a promoter of cell adhesion and activation. The quality of this biofilm layer is influenced by the implant surface properties [13,14].

The role played by the adsorbed proteins is crucial in the healing process. It has been reported, in fact, that fibrinogen initiates the acute inflammatory response which follows the implant placement,

thus being actively involved in the bone healing process [15]. Moreover, fibrinogen, which together with the protein cascade is activated by the contact between plasma and titanium surface [16–20], is decisive for the fibrin activation which leads to the fibrin clot formation [21].

At the same time, in the injury site, the fibrin network supports the initial endothelial response providing a transitory matrix [22]. Fibrin turnover is a very rapid process [23]: In a few minutes factor XIII induces the fibrin monomers polymerization which causes the creation of a tight structure [24]. The process starts with the formation of a thrombus on the biomaterial surface due to electric charges transfer from the inactive fibrinogen to the above-mentioned surface [25]. The contact between fibrinogen and titanium surface oxide film produces a junction by electronic transfer which improves the blood compatibility of the titanium [25] and allows cells to interact with a blood-oxide-titanium modified surface [26]. On the other hand, the surface roughness of the titanium is also significantly related to the fibrin clot retention [27] and influences the cellular response. Cytoskeleton appears to be highly sensitive to intermediate level of roughness [8]. Grit-blasted and acid-etched surfaces have shown a higher percentage of bone-implant contact (*BIC*) in the early period (4 weeks) compared to grit-blasted surfaces alone, although no statistically significant difference has been found between the groups after 12 weeks of healing [28]. However, grit-blasted and acid-etched procedures create different roughness and oxide thickness [28]. It has been also demonstrated that *BIC* increases as the surface become rougher [29,30]. Several studies [31–35] have reported a significant relationship between *BIC* and oxide thickness of the titanium, thus highlighting the importance of titanium oxidation treatments [36]. In particular, a better bone-implant surface reaction is allowed by an oxide film thickness of 600–1000 nm [36]. Various methods have been introduced in order to modify the surface oxide film properties and enhance the biocompatibility of titanium implants and the osseointegration process. A number of studies have demonstrated that the modified surface oxides improve the bone response, at least in animal models. However, the specific effects on bone response are largely unknown [37–42].

Among all these methods, anodic electrochemical oxidation offers the opportunity to control the oxide properties, which are strongly dependent on the electrochemical parameters chosen. The surface topography at the ultrastructural level is the result of the field-assisted migration of ions throughout the oxide film, while the thickness of the anodic oxide follows the Faraday's Law [43]. The anodization technique increases the surface roughness of titanium since it creates a thick oxide layer (1500 nm) [44], with a crystalline phase consisting principally of anatase  $\text{TiO}_2$  [45] and characterized by micro pores and nanotube arrays [46,47]. This higher roughness, together with a lower water contact angle and thus a wettability increase, results in a hydroxylated and hydrophilic surface which supports the adhesion of suitable proteins [44] and enhances the early stage of osseointegration [48]. In other terms, the anodization process is thought to improve the osteoblasts reaction responsible for the osseointegration process between the titanium surface and the surrounding bone, thus providing an accelerated bioactivity that may be recommended for early loading [49,50].

From this perspective, the aims of this study were to investigate the fibrin clot extension associated to the contact angle, the micro and nano-scale roughness between anodized and non-anodized titanium surfaces and report the *BIC* rate of two narrow one-piece dental implants recovered due to fracture.

The null hypothesis under test considers that an anodized titanium surface shows no difference in rate for *bce*,  $R_a$ ,  $\theta$  or *BIC* rather than a not anodized titanium surface.

## 2. Materials and Methods

### 2.1. Specimen Preparation

A total of 34 flat pentagonal grade V titanium specimens were used in the in-vitro study (Figure 1). The samples surfaces were grit-blasted with 180  $\mu\text{m}$  aluminum oxide at 0.25 MPa producing *Ra* values ranging between 1.5 and 2.5  $\mu\text{m}$  and acid-etched in a solution of 5 N  $\text{HNO}_3$  and 5 N HF at room temperature (20 °C) for 20 min. Half of these samples were subsequently subjected to the anodizing

process in an anodizing bath heated at 20 °C of 1.0 M phosphoric acid under a current density of 5 mA·cm<sup>-2</sup> due to a stabilized current of 80 V (Figure 1A). The anodizing process resulted in the formation of an oxide layer with a thickness of 120 μm in about 30 s.

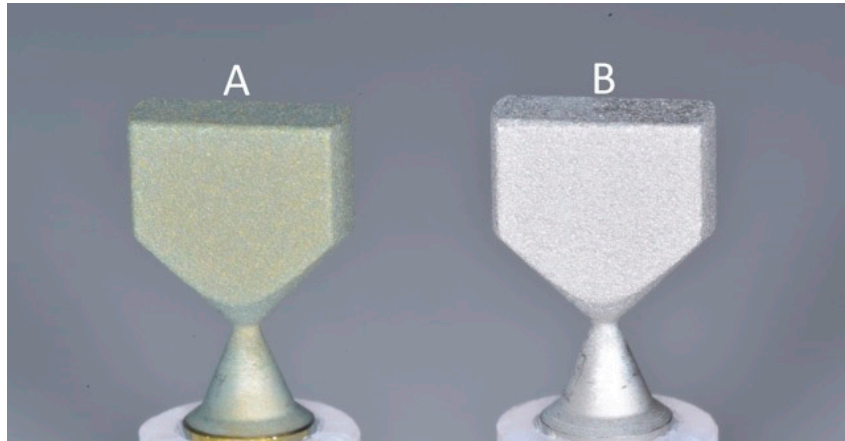


**Figure 1.** Titanium specimens prepared for the in-vitro tests, after grit-blasting and acid-etching: (A) test sample with anodization; (B) control sample without anodization.

## 2.2. Contact Angle ( $\theta$ ) Measurement

8 samples were used to measure the contact angle (4 with anodized surface and 4 without).

Static contact angles, i.e., the angle between the tangent to a water drop and the solid surface at the three-phase liquid-solid-air meeting point was used as a measure of the surface hydrophobicity.

A water drop of 10 μL of volume was placed over each one of the titanium specimens in the same environmental conditions (Figure 2). The contact angle was measured using physiological solution instead of distilled water in order to have the same osmolarity of the blood. The contact angle was measured using ImageJ 1.47v (National Institute of Health, Bethesda, MD, USA), with the plugin named drop analysis-LB-ADSA (Biomedical Imaging Group, EPFL, Lausanne, Switzerland). The measuring procedure followed a preliminary image processing aimed at improving the contrast of the image. The images obtained in RGB colors were split into the three channels: red; green and blue, each one at 8 bit. Only the blue channel of the converted images was used for the drop analysis measurement. The contact angle value for each specimen was calculated both for left and right side and reported as a mean of each specimen.



**Figure 2.** Contact angle measurement with 10 μL of physiological solution: (A) Test and (B) control.

### 2.3. Blood Clot Extension (bce) Measurement

Blood clot extension was measured on 14 samples (7 with anodization and 7 without). 10  $\mu$ L of venous blood were drawn from one healthy adult male voluntary not on medication and with a bleeding time between 2 and 3 min (Duke's essay). A drop of whole blood without any addition of anticoagulant was immediately placed onto the surface of each specimen using a syringe (Hamilton Company, Bonaduz, Switzerland) (Figure 3). Contact time was 5 min at the room temperature; specimens were then rinsed with saline solution and fixed in a buffered solution of 2.5% of glutaraldehyde and paraformaldehyde at pH 7.2. Samples were washed again in a saline solution and dehydrated in an ascending alcohol series of 50%, 70%, 90%, 95%, and 100%. After dehydration, the specimens were treated in a critical point drying (Emitech K850 critical point dryer, Ashford, Kent, UK), mounted onto aluminum stubs and gold coated with a Emitech K550 sputter coater. SEM observations were carried out by the use of a SEM.

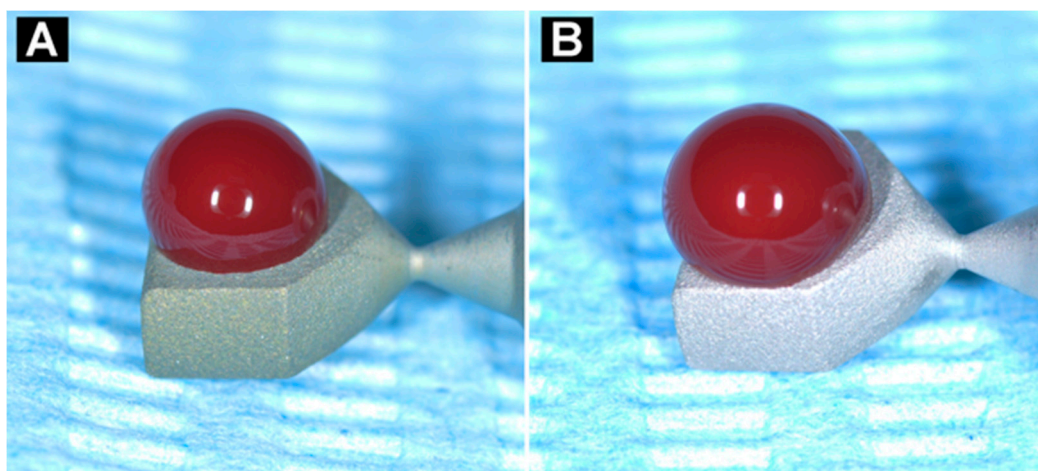


**Figure 3.** Blood clot test using 10  $\mu$ L of human venous blood with contact time of 5 min at room temperature. In (A) test specimen and control specimens in (B).

### 2.4. SEM Observation

Samples were observed using a scanning electron microscope (SEM) with LaB6 electron beam (Zeiss EVO 50 XVP, Carl Zeiss SMY Ltd., Cambridge, UK), equipped with tetra solid-state back scattered electrons (BSE) detector (Figure 4A,B). SEM operating conditions included 10 kV accelerating voltage, 10 mm working distance and 1.2 mA probe current. The observations were made under variable pressure at 0.75 torr using both BSE and SE1 detectors. Images were captured with a line average technique using 20 scans. To measure the fibrin clot extension, images at 39 $\times$  magnification were used. The fibrin clot was measured using ImageJ Software 1.47v.

To elude artifacts, the sample surfaces of the images were cut to eliminate the background. The resampled images were converted in 32 bit, then, using the threshold function of the software, the region of interest (ROI) related to the samples surface covered by the clot and free titanium surface were selected. The ROIs were evaluated with the automatic function of the software in square pixel and collected. Measurements were triplicate and reported as mean value ( $\pm$ SD) to control the variability of the technique.

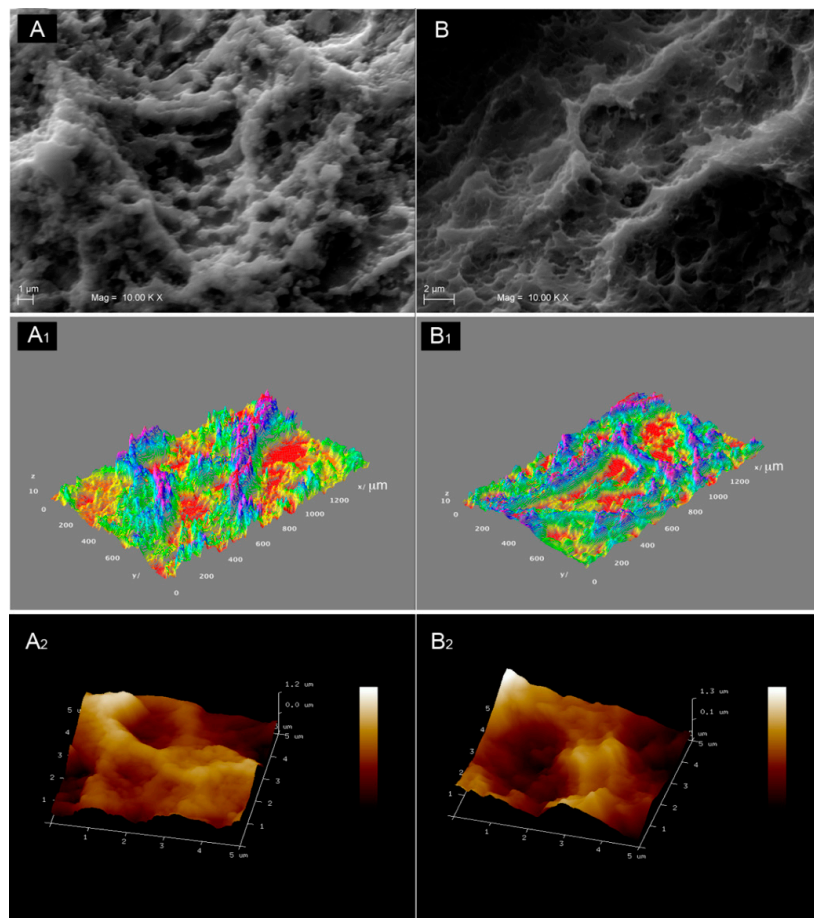


**Figure 4.** SEM images at 10,000 $\times$  magnifications of the surfaces of the specimens and 3D surface plots reconstructions; In (A) specimen of the test group with the characteristic nodular surface, In (B) specimen of the control group without nodules; In (A<sub>1</sub>,B<sub>1</sub>) the 3D reconstruction at microscale level of the  $R_a$  values measured under CLSM of test and control specimens respectively; In (A<sub>2</sub>,B<sub>2</sub>) 3D representation at nanoscale level of the  $R_a$  measured under AFM.

### 2.5. Surface Micro-Roughness ( $R_a$ )

The surface roughness at micro-scale level was measured by a means of a Zeiss confocal laser scanning microscope (CLSM) 510 META (Zeiss, Jena, Germany) using a 15-mV argon laser with an objective of 40 $\times$ /1.2 numerical aperture (NA). A total of 6 samples were used (3 with anodization and 3 without). For each specimen, three surface ROIs of 0.6 mm  $\times$  1.2 mm were evaluated. The parameter measured was the average height deviation value ( $R_a$ ).

### 2.6. Surface Nano-Roughness ( $R_a$ )

The surface roughness at nano-scale level was evaluated using an atomic force microscope (AFM) MultiMode 8 AFM with a NanoScope V controller (Bruker, Santa Barbara, CA, USA). The AFM setting included ScanAsyst Mode, which performs automatic image optimization, based on PeakForce Tapping™ technology, which directly controls the tip-sample interaction force. The scan size was set at 500 nm with a scan rate of 1 Hz, and a peak force set point of 0.060 V for a Z range of 9.5  $\mu$ m (Figure 4). A total of 6 samples were used (3 with anodization and 3 without). Three surface ROIs of 5  $\mu$ m  $\times$  5  $\mu$ m were evaluated for each specimen. The parameter measured was the average height deviation value ( $R_a$ ).

### 2.7. Implant Retrieval and Evaluation

Two one-piece narrow (2.8 mm × 10 mm) Ti6Al4V dental implants (KOS micro Implants, IDHE Dental AG, Gommiswold, Switzerland), and the surrounding hard tissues were retrieved for fracture of the implant neck. The not anodized implant (#36) fractured spontaneously after 8 months of functional prosthetic loading, while the anodized implant (#35) remained in function two additional months as support for the crowns (#35, #36), the fracture happened during the removal of the prosthesis. Both implants were located in the posterior region of the mandible of the same patient: A 55-year-old man. The implants were placed to support a long-term interim metal and resin fixed prosthesis made by two connected elements. Both of these implants were stable before removal and did not suffer from any infection; the implant fragments were removed using a 5Ø mm trephine bur (Henry Schein Krugg Buccinasco, Milan, Italy).

### 2.8. Specimen Processing

The retrieved implants were carefully rinsed with a cold 5% glucose solution to remove blood while maintaining the correct osmolarity (278 mOsm·L<sup>-1</sup>).

The specimens were fixed in 10% formalin solution at pH 7.2 for a week and dehydrated with a graded series of alcohols. After pre-infiltration treatment in a 50% resin/alcohol solution (Technovit 7200 VLC, Kulzer, Hanau, Germany) for ten days, the specimens were easily removed from the trephine burs with a custom-made plunger and completely embedded in 100% resin. Finally, the specimens were oriented and polymerized. A high-precision cutting system (TT System, TMA2, Grottammare, Italy) with a diamond disc was used to prepare two sections of the specimens along the longitudinal axis of about 50 µm in thickness. The sections were subsequently ground to about 30 ± 10 µm under running water with a series of polishing discs, followed by a final polish with 0.1 µm of alumina particles in a microgrinding system (TT System, TMA2, Grottammare, Italy). The prepared sections were not stained. The investigation was conducted in a circularly polarized light microscope (BX 51, Olympus America, Center Valley, PA, USA) connected to a high-resolution digital camera (FinePix S2 Pro, Fuji Photo Film, Tokyo, Japan). The histomorphometric analysis was performed by means of a software package with image capturing capabilities (Image-Pro Plus 6.0, Media Cybernetics Inc., Bethesda, Rockville, MD, USA) by a trained and experienced operator (TT). To ensure accuracy, the software was calibrated for each experimental image using “Calibration Wizard”, a feature that reports the number of pixels between two selected points of a micrometer scale. The linear remapping of the pixel numbers in microns was used to calibrate the distance.

For the histomorphometric evaluation, the bone-to-implant contact (*BIC*%), defined as the amount of mineralized bone in direct contact with the implant surface, was measured around all implant surfaces in two sections obtained from each specimen. Means and standard deviations of *BIC*% were calculated for each implant and then compared.

### 2.9. Statistics

Statistical analysis was performed by means of a computerized statistical package (Sigma Stat 3.5, SPSS Inc., Ekrath, Germany). Data normality was tested with Shapiro-Wilk test and Q-Q normality plots of the residuals, and equality of variance among the datasets by using a Levene test. All datasets met the required assumptions for using parametric methods. Student t-test analysis was used to evaluate the significance between groups, moreover, correlations between blood clot extensions, contact angles, micro-roughness and nano-roughness were searched using a bivariate Pearson correlation test. A *p*-value of <0.05 was considered statistically significant.

### 3. Results

#### 3.1. Contact Angle

Contact angle measured as  $\theta$  ( $n = 8$ ) showed a mean value ( $\pm$ SD) of  $98.5^\circ$  ( $\pm 18.7^\circ$ ) for the test group and  $103^\circ$  ( $\pm 15.2^\circ$ ) for the control group. The difference between the two groups of  $-4.52^\circ$  appeared to be not statistically significant different ( $p = 0.507$ ) (Figure 2).

#### 3.2. Micro-Roughness

The micro-roughness measured as  $R_a$  value ( $n = 6$ ) was for the test group  $6.0$  ( $\pm 1.5$ )  $\mu\text{m}$  and for the control group was  $5.8$  ( $\pm 1.8$ )  $\mu\text{m}$ . The difference between the two groups of  $0.2$   $\mu\text{m}$  was not statistically significant different ( $p = 0.248$ ) (Figure 4A<sub>1</sub>,B<sub>1</sub>).

#### 3.3. Nano-Roughness

The nano-roughness measured as  $R_a$  value ( $n = 6$ ) was for the test group  $286$  ( $\pm 40$ ) nm and for the control group was  $226$  ( $\pm 40$ ) nm. The difference between the two groups of  $60$  nm was statistically significant different ( $p = 0.029$ ) (Figure 4A<sub>2</sub>,B<sub>2</sub>).

#### 3.4. Blood Clot Extension

The fibrin clot extensions measured as surface percentage in  $\text{pixel}^2$  ( $n = 14$ ). Showed for test group a mean value ( $\pm$ SD) of  $42.5\%$  ( $\pm 22\%$ ) while the control group reported  $26.6\%$  ( $\pm 13\%$ ). The difference between the groups of  $15.9\%$  was statistically significant different ( $p = 0.049$ ) (Figures 5 and 6).

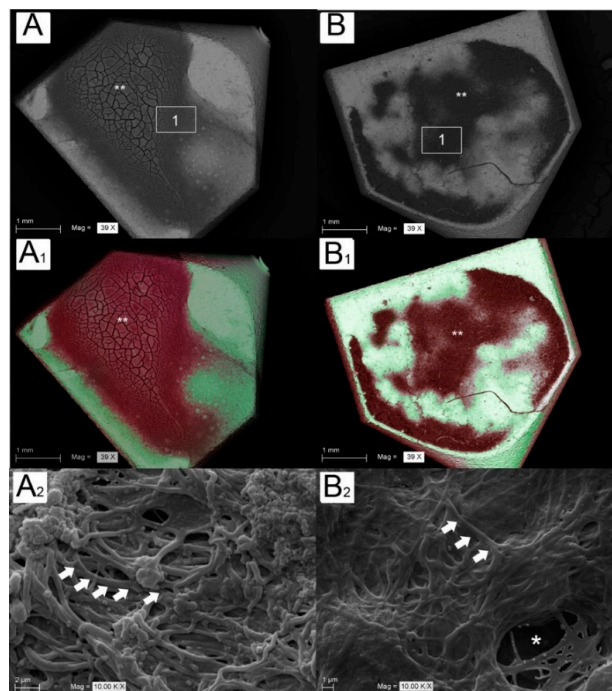


**Figure 5.** SEM images at  $39\times$  magnifications of the fibrin clot over the surfaces of the specimens. In (A,A<sub>1</sub>) specimen of the test group with fibrin clot (\*\*) in evidence respect to the titanium pseudocolored in green in (A<sub>1</sub>). The square rectangle 1 imaged at  $10,000\times$  magnifications in (A<sub>2</sub>) shows the fibrin filaments (white arrows) well organized and represented over the surface of the test specimen. In (B,B<sub>1</sub>) specimen of the control group with fibrin clot (\*\*) in evidence respect to the titanium pseudocolored in green in (B<sub>1</sub>). The square rectangle 1 imaged at  $10,000\times$  magnifications in (B<sub>2</sub>) shows a lesser amount of the fibrin filaments (white arrows) over the titanium surface of the control specimen which appeared in part visible (\*).

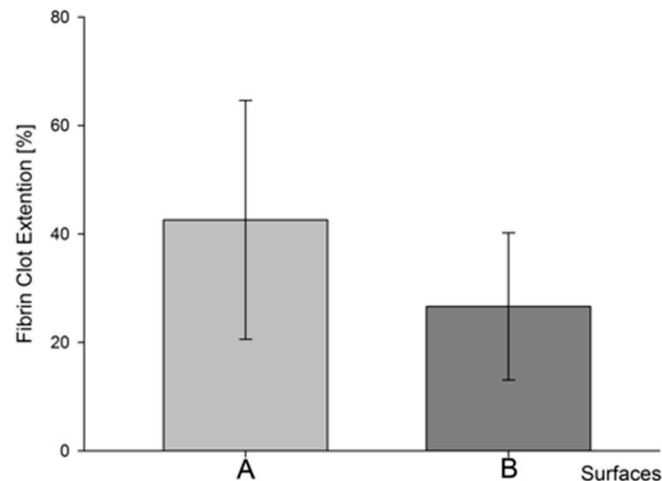


**Figure 6.** Graphical representation of fibrin clot extension rate (%) versus surfaces. In (A) the test group; in (B) the control group. The difference between groups was statistically significant ( $p = 0.049$ ); (two tailed unpaired  $t$ -test).

Under SEM observation the fibrin clot appeared not uniformly distributed over the surfaces of the samples (Figure 5A<sub>1</sub>,B<sub>1</sub>). On some specimens of both groups the fibrin was organized as a single spot with irregular shape, while in some other adhered with a multi-spot arrangement.

### 3.5. Bivariate Pearson Correlation

The linear relationships between variables and strength of linkage in a single value ( $R$ ) between  $-1$  and  $+1$  was used.

A positive  $R$  value expresses a positive relationship between the two considered variables while a negative  $R$  value indicates a negative relationship. A correlation coefficient of zero indicates no relationship between the variables at all. Contact angle to blood clot extension  $R = -0.263$  ( $p = 0.6$ ), contact angle to nano-roughness  $R = -0.864$  ( $p = 0.026$ ), contact angle to micro-roughness  $R = 0.193$  ( $p = 0.70$ ) (Figure 7).

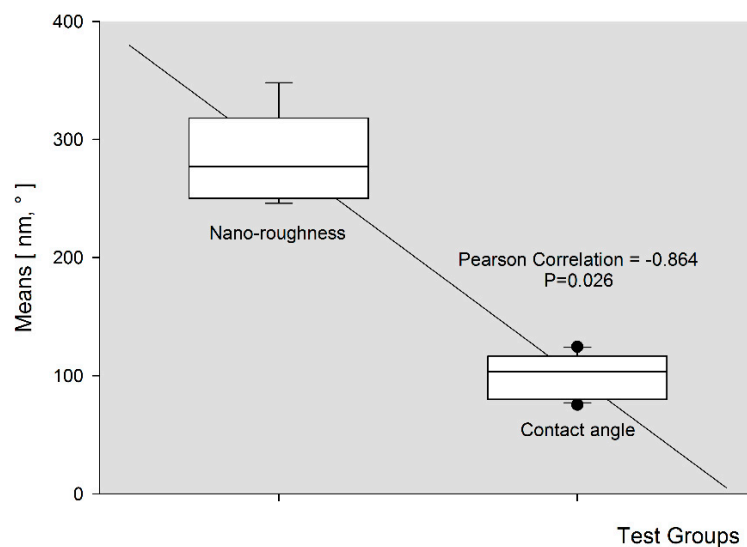


**Figure 7.** Graphical representation of bivariate Pearson correlation of the means ( $\pm$ SD) of the contact angle ( $\theta$ ) versus nano-roughness ( $R_a$ ) of the test group. The two variables appeared significantly correlated ( $p = 0.026$ ) with a negative coefficient ( $R = -0.864$ ).

### 3.6. Histomorphometric Evaluation

The anodized implant showed a prevalent lamellar bone in direct contact to the implant surface. This aspect indicates a contact osteogenesis process in which osteoprogenitor cells colonize on the implant surface and differentiate into mature, bone forming osteoblasts. Conversely, the control group showed several areas of marrow spaces contacting the implant surface, indicating a distance osteogenesis ingrowth of bone from the lateral walls of the osteotomy (Figure 8).

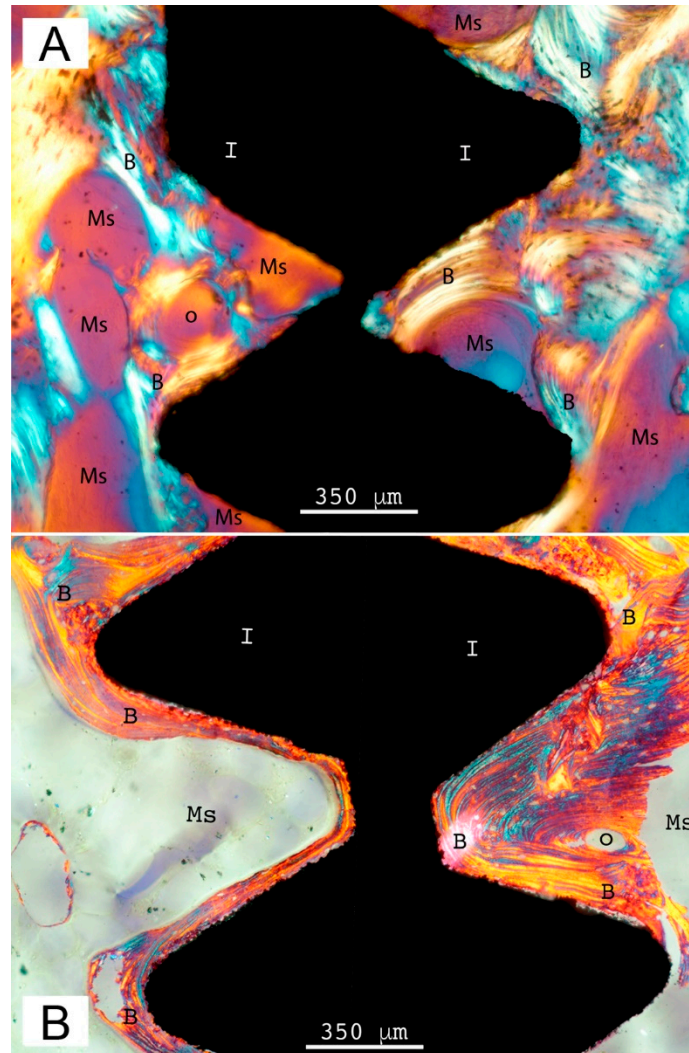


**Figure 8.** Histological sections of fractured implants under circularly polarized light microscope. Original magnification 200 $\times$ . In (A), the not anodized implant (control) after 8 months of load. The bone (B) appear to be in contact with the implant surface (I) in several areas, as well as, several marrow spaces (Ms) appear to be in contact with the implant surface. An osteon (O) was present between two threads but in the context of a bone trabecula. In general, the bone around not anodized implant was formed by a distance osteogenesis: this is deduced from the presence of several marrow spaces contacting the implant surface. Conversely, in (B) the anodized implant (test) after 10 months of load showed a lamellar bone contacting completely the implant surface (I). An osteon (o) was visible between two threads. Finally, in the anodized implant, the marrow spaces were not in contact with the implant. Around anodized implants the bone was formed by a contact osteogenesis.

The BIC rate were 34.5% ( $\pm 2.1\%$ ) for control implant (not anodized) and 52.5% ( $\pm 2.1\%$ ) for test implant (anodized). A statistically significant difference was present ( $p = 0.014$ ) (Figure 9).

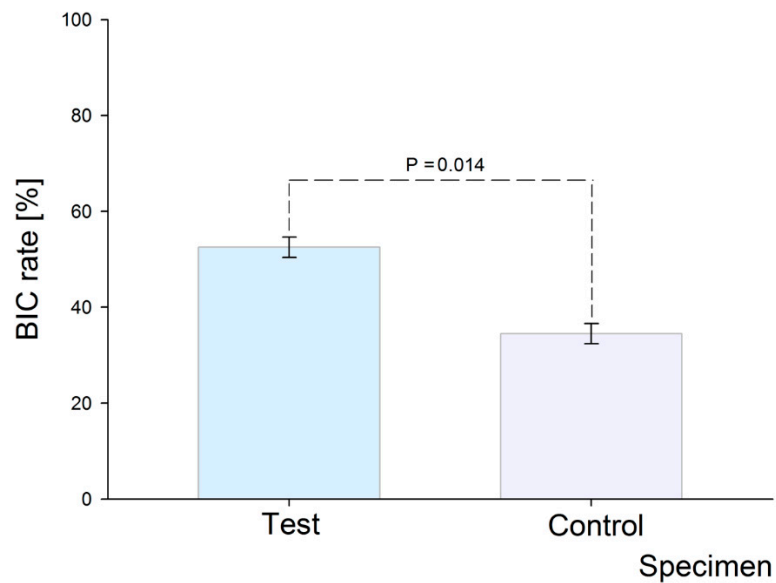


**Figure 9.** Graphical representation of *BIC* rate (%) versus surfaces. The difference between test and control groups was statistically significant ( $p = 0.014$ ); (two tailed unpaired *t*-test).

#### 4. Discussion

Within the limitations of the study, the null hypothesis under test was rejected for *bce*, *BIC* rate and nano- $R_a$ , while we fail to reject the null hypothesis for  $\theta$  and micro- $R_a$ .

In fact, experimental results showed significant differences for fibrin clot extension between test (anodized) and control (not anodized) specimens. At the same time, no differences were found for contact angle and surface micro-roughness. Meanwhile, the nano-roughness showed a statistically significant difference.

The bivariate correlation showed a significant negative strong contribution of nano-roughness over the micro-roughness on fibrin clot adhesion to anodized titanium surface.

Despite this, there are many factors that are considered primary in the early phases of the healing process around dental implants.

Osteogenic cell migration and de novo bone formation directly onto the implant surface require a transitory matrix, mainly represented by the fibrin scaffold [1].

Within the limitation of the present single case report, the histological evaluation conserves the power of an in-vivo human observation. Other interesting factors include the adjacent sites for test and control implants on the same patient and the placement of the implants in normal function for eight months with a definitive prosthesis. Anodized titanium surface, by promoting the blood clot formation at early stage, improves at the same time the quality and the quantity of the osseointegration process. The osteoprogenitor cells, in presence of a well-structured and spread transitory matrix formed by the fibrin clot, can easily colonize the implant surface. After that, the cells can differentiate into mature bone forming osteoblasts, starting the contact osteogenesis process, which improve the *BIC* rate. Conversely, the control group showed a distance osteogenesis ingrowth since several areas of marrow spaces were in contact to the implant surface.

It appears evident that wider is the extension of clot retained on implant surface, better is the healing process and osseointegration; this could be particularly useful in clinical situations where immediate loading is requested.

It is commonly accepted that the best implant surfaces are those which have the highest surface energy, as they maximize blood contact and therefore healing. However, the results of this study could suggest that there is no real relationship between the amount of surface energy and the binding of fibrin onto implant surface.

This could change the research approach on the new surfaces, focusing on the chemical interactions and reactions to blood.

Both in vitro [38,39] and in vivo studies [40,41] reported a positive correlation between fibrin adhesion and surface wettability. Fibrin adhesion is influenced by different parameters: Blood drop extension, gravity of the drop, liquid characteristics, and thermodynamics aspects [42]. The most used parameters to evaluate wettability are contact angle (water contact angle (WCA) and surface tension. In liquids, increasing wettability causes decreasing surface tension [42]. Water surface tension is  $\sim 73 \text{ mNm}^{-1}$  in contrast to blood that has  $52 \text{ mN}\cdot\text{m}^{-1}$  at  $37^\circ\text{C}$  [44]. For this reason, Vogler ascribed to adhesion tension (wetting tension) a more predictive role for biological responses than to other surface energy parameters [45]. It has been reported that increased surface hydrophilicity increases the likelihood of cell adhesion to the surface [46,47]. So, it results that surface chemistry is the dominant parameter governing surface properties [48]. This suggests that implant surface could be conditioned by different procedures. It is shown that both organic and inorganic impurities on the surface can increase WCA, so different decontamination techniques were investigated [49]. On titanium surface exposed to UV-A treatment was observed a superhydrophilicity behavior, due to an increased anatase surface modifications [50].

The Wenzel theory says that a wetting liquid completely fills a rough surface topography, including all indentations and pores [51]. Enhancing surface roughness increases hydrophilicity in hydrophilic surfaces and hydrophobicity of hydrophobic surfaces.

The presence of numerous pores on the surface can show a hydrophobic behavior cause the air in the pores don't allow the liquid penetrations, it changes when pores are interconnected so the air can exit, increasing the wettability [52,53]. For this reason, several conservation techniques of implants have been introduced. Good wettability is demonstrated on titanium surface treated with nitrogen after blasting-acid etching (BAE) procedures and stored in neutral saline solution [54,55].

It has been demonstrated as anodization increases the surface characterization, making titanium samples rougher thanks to nanotube formation. This increases the surface energy and wettability inducing a higher osteoblast adhesion and fibronectin and vitronectin cell expression [56].

In our study a significant negative strong correlation was identified between contact angle and nano-roughness but not with micro-roughness. This could suggest that surface energy and wettability may not be strongly correlated to a fibrin adhesion improvement.

This could induce better investigation on the chemical and electric surface characteristics of implants and their relationships.

## 5. Conclusions

Within the limit of the study, the anodized titanium surface demonstrates a high ability to induce the fibrin adhesion, which in turn correlate to the increase of nano-roughness. At the same time the anodized dental implants, after 10 months of load, showed a *BIC* rate significantly higher compared to non-anodized implants.

**Author Contributions:** Conceptualization, T.T.; Methodology, G.P.; Formal Analysis, B.S.; Investigation, T.T.; Resources, T.T.; Data Curation, G.M.; Writing-Review & Editing, T.T. and A.S.; Visualization, C.D.; Supervision, S.C.

**Funding:** This research was funded by Tonino Traini ex 60% University of Chieti funds.

**Acknowledgments:** We are grateful to BIOMED Implant–Niba FD s.r.l. for the specimens preparation.

**Conflicts of Interest:** The authors declare no conflict of interest.

## References

1. Davies, J.E. Mechanisms of endosseous integration. *Int. J. Prosthodont.* **1998**, *11*, 391–401. [[PubMed](#)]
2. Anderson, J.M. Biological Responses to Materials. *Annu. Rev. Mater. Res.* **2001**, *31*, 81–110. [[CrossRef](#)]
3. Arvidsson, S.; Askendal, A.; Tengvall, P. Blood plasma contact activation on silicon, titanium and aluminium. *Biomaterials* **2007**, *28*, 1346–1354. [[CrossRef](#)] [[PubMed](#)]
4. Albrektsson, T.; Branemark, P.I.; Hansson, H.A.; Lindstrom, J. Osseointegrated titanium implants. Requirements for ensuring a long-lasting, direct bone-to-implant anchorage in man. *Acta Orthop. Scand.* **1981**, *52*, 155–170. [[CrossRef](#)] [[PubMed](#)]
5. Magnani, A.; Priamo, A.; Pasqui, D.; Barbucci, R. Cell behaviour on chemically microstructured surfaces. *Mater. Sci. Eng. C* **2003**, *23*, 315–328. [[CrossRef](#)]
6. Riehle, M.O.; Dalby, M.J.; Johnstone, H.; MacIntosh, A.; Affrossman, S. Cell behaviour of rat calvaria bone cells on surfaces with random nanometric features. *Mater. Sci. Eng. C* **2003**, *23*, 337–340. [[CrossRef](#)]
7. Karacs, A.; Joob Fancsaly, A.; Divinyi, T.; Pető, G.; Kovách, G. Morphological and animal study of titanium dental implant surface induced by blasting and high intensity pulsed Nd-glass laser. *Mater. Sci. Eng. C* **2003**, *23*, 431–435. [[CrossRef](#)]
8. Lange, R.; Lüthen, F.; Beck, U.; Rychly, J.; Baumann, A.; Nebe, B. Cell-extracellular matrix interaction and physico-chemical characteristics of titanium surfaces depend on the roughness of the material. *Biomol. Eng.* **2002**, *19*, 255–261. [[CrossRef](#)]
9. Keselowsky, B.G.; Collard, D.M.; García, A.J. Surface chemistry modulates focal adhesion composition and signaling through changes in integrin binding. *Biomaterials* **2004**, *25*, 5947–5954. [[CrossRef](#)] [[PubMed](#)]
10. Gorbet, M.B.; Sefton, M.V. Biomaterial-associated thrombosis: Roles of coagulation factors, complement, platelets and leukocytes. *Biomaterials* **2004**, *25*, 5681–5703. [[CrossRef](#)] [[PubMed](#)]
11. Smith, B.R.; Rinder, H.M.; Rinder, C.S. Interaction of blood and artificial surfaces. In *Thrombosis and Hemorrhage*, 3rd ed.; Loscalzo, J., Schafer, A.I., Eds.; Lippincott Williams & Wilkins: Philadelphia, PA, USA, 2003; pp. 865–900.
12. Nygren, H.; Tengvall, P.; Lundstrom, I. The initial reactions of TiO<sub>2</sub> with blood. *J. Biomed. Mater. Res.* **1997**, *34*, 487–492. [[CrossRef](#)]
13. Horbett, T.A. Chapter 13 Principles underlying the role of adsorbed plasma proteins in blood interactions with foreign materials. *Cardiovasc. Pathol.* **1993**, *2*, 137–148. [[CrossRef](#)]
14. Vroman, L. Problems in the development of materials that are compatible with blood. *Biomater. Med. Devices Artif. Organs* **1984**, *12*, 307–323. [[CrossRef](#)] [[PubMed](#)]
15. Tang, L.; Eaton, J.W. Fibrin(ogen) mediates acute inflammatory responses to biomaterials. *J. Exp. Med.* **1993**, *178*, 2147–2156. [[CrossRef](#)] [[PubMed](#)]
16. Bangham, A.D. A Correlation between Surface Charge and Coagulant Action of Phospholipids. *Nature* **1961**, *192*, 1197–1198. [[CrossRef](#)] [[PubMed](#)]
17. Jackson, C.M.; Nemerson, Y. Blood coagulation. *Annu. Rev. Biochem.* **1980**, *49*, 765–811. [[CrossRef](#)] [[PubMed](#)]
18. Drummond, R.K.; Peppas, N.A. Fibrinolytic behaviour of streptokinase-immobilized poly(methacrylic acid-g-ethylene oxide). *Biomaterials* **1991**, *12*, 356–360. [[CrossRef](#)]
19. Siemssen, P.A.; Garred, P.; Olsen, J.; Aasen, A.O.; Mollnes, T.E. Activation of Complement Kallikrein-kinin, Fibrinolysis and Coagulation Systems by Urinary Catheters. Effect of Time and Temperature in Biocompatibility Studies. *Br. J. Urol.* **1991**, *67*, 83–87. [[CrossRef](#)] [[PubMed](#)]
20. Johnson, R.J. Complement activation during extracorporeal therapy: Biochemistry, cell biology and clinical relevance. *Nephrol. Dial. Transplant.* **1994**, *9*, 36–45. [[PubMed](#)]
21. Mosesson, M.W. Fibrinogen functions and fibrin assembly. *Fibrinolysis Proteolysis* **2000**, *14*, 182–186. [[CrossRef](#)]
22. Kawase, T.; Okuda, K.; Wolff, L.F.; Yoshie, H. Platelet-rich plasma-derived fibrin clot formation stimulates collagen synthesis in periodontal ligament and osteoblastic cells in vitro. *J. Periodontol.* **2003**, *74*, 858–864. [[CrossRef](#)] [[PubMed](#)]
23. Schmoekel, H.; Schense, J.C.; Weber, F.E.; Grätz, K.W.; Gnägi, D.; Müller, R.; Hubbell, J.A. Bone healing in the rat and dog with nonglycosylated BMP-2 demonstrating low solubility in fibrin matrices. *J. Orthop. Res.* **2004**, *22*, 376–381. [[CrossRef](#)]

24. Yucel, E.A.; Oral, O.; Olgac, V.; Oral, C.K. Effects of fibrin glue on wound healing in oral cavity. *J. Dent.* **2003**, *31*, 569–575. [[CrossRef](#)]
25. Chen, J.Y.; Leng, Y.X.; Tian, X.B.; Wang, L.P.; Huang, N.; Chua, P.K.; Yang, P. Antithrombogenic investigation of surface energy and optical bandgap and hemocompatibility mechanism of Ti(Ta<sup>+5</sup>)O<sub>2</sub> thin films. *Biomaterials* **2002**, *23*, 2545–2552. [[CrossRef](#)]
26. Park, J.Y.; Gemmell, C.H.; Davies, J.E. Platelet interactions with titanium: Modulation of platelet activity by surface topography. *Biomaterials* **2001**, *22*, 2671–2682. [[CrossRef](#)]
27. Di Iorio, D.; Traini, T.; Degidi, M.; Caputi, S.; Neugebauer, J.; Piattelli, A. Quantitative evaluation of the fibrin clot extension on different implant surfaces: An in vitro study. *J. Biomed. Mater. Res. B Appl. Biomater.* **2005**, *74*, 636–642. [[CrossRef](#)] [[PubMed](#)]
28. Kim, Y.H.; Koak, J.Y.; Chang, I.T.; Wennerberg, A.; Heo, S.J. A histomorphometric analysis of the effects of various surface treatment methods on osseointegration. *Int. J. Oral Maxillofac. Implant.* **2003**, *18*, 349–356.
29. Buser, D.; Schenk, R.K.; Steinemann, S.; Fiorellini, J.P.; Fox, C.H.; Stich, H. Influence of surface characteristics on bone integration of titanium implants. A histomorphometric study in miniature pigs. *J. Biomed. Mater. Res.* **1991**, *25*, 889–902. [[CrossRef](#)] [[PubMed](#)]
30. Larsson, C.; Thomsen, P.; Lausmaa, J.; Rodahl, M.; Kasemo, B.; Ericson, L.E. Bone response to surface modified titanium implants: Studies on electropolished implants with different oxide thicknesses and morphology. *Biomaterials* **1994**, *15*, 1062–1074. [[CrossRef](#)]
31. Albrektsson, T.; Johansson, C.; Lundgren, A.; Sul, Y.; Gottlow, J. Experimental studies on oxidized implants. A histomorphometrical and biomechanical analysis. *Appl. Osseointegr. Res.* **2000**, *1*, 21–24.
32. Nishiguchi, S.; Kato, H.; Fujita, H.; Kim, H.M.; Miyaji, F.; Kokubo, T.; Nakamura, T. Enhancement of bone-bonding strengths of titanium alloy implants by alkali and heat treatments. *J. Biomed. Mater. Res. Part A* **1999**, *48*, 689–696. [[CrossRef](#)]
33. Larsson, C.; Thomsen, P.; Aronsson, B.-O.; Rodahl, M.; Lausmaa, J.; Kasemo, B.; Ericson, L.E. Bone response to surface-modified titanium implants: Studies on the early tissue response to machined and electropolished implants with different oxide thicknesses. *Biomaterials* **1996**, *17*, 605–616. [[CrossRef](#)]
34. Hazan, R.; Brener, R.; Oron, U. Bone growth to metal implants is regulated by their surface chemical properties. *Biomaterials* **1993**, *14*, 570–574. [[CrossRef](#)]
35. Fini, M.; Cigada, A.; Rondelli, G.; Chiesa, R.; Giardino, R.; Giavaresi, G.; Nicoli Aldini, N.; Torricelli, P.; Vicentini, B. In vitro and in vivo behaviour of Ca- and P-enriched anodized titanium. *Biomaterials* **1999**, *20*, 1587–1594. [[CrossRef](#)]
36. Sul, Y.-T.; Johansson, C.B.; Röser, K.; Albrektsson, T. Qualitative and quantitative observations of bone tissue reactions to anodised implants. *Biomaterials* **2002**, *23*, 1809–1817. [[CrossRef](#)]
37. Durual, S.; Pernet, F.; Rieder, P.; Mekki, M.; Cattani-Lorente, M.; Wiskott, H.W. Titanium nitride oxide coating on rough titanium stimulates the proliferation of human primary osteoblasts. *Clin. Oral Implant. Res.* **2011**, *22*, 552–559. [[CrossRef](#)] [[PubMed](#)]
38. Massa, M.A.; Covarrubias, C.; Bittner, M.; Fuentevilla, I.A.; Capetillo, P.; Von Marttens, A.; Carvajal, J.C. Synthesis of new antibacterial composite coating for titanium based on highly ordered nanoporous silica and silver nanoparticles. *Mater. Sci. Eng. C Mater. Biol. Appl.* **2014**, *45*, 146–153. [[CrossRef](#)] [[PubMed](#)]
39. Souza, F.A.; Queiroz, T.P.; Sonoda, C.K.; Okamoto, R.; Margonar, R.; Guastaldi, A.C.; Nishioka, R.S.; Garcia Júnior, I.R. Histometric analysis and topographic characterization of cp Ti implants with surfaces modified by laser with and without silica deposition. *J. Biomed. Mater. Res. B Appl. Biomater.* **2014**, *102*, 1677–1688. [[CrossRef](#)] [[PubMed](#)]
40. Mazzola, L.; Bemporad, E.; Misiano, C.; Pepe, F.; Santini, P.; Scandurra, R. Surface analysis and osteoblasts response of a titanium oxo-carbide film deposited on titanium by ion plating plasma assisted (IPPA). *J. Nanosci. Nanotechnol.* **2011**, *11*, 8754–8762. [[CrossRef](#)] [[PubMed](#)]
41. Maho, A.; Linden, S.; Arnould, C.; Detriche, S.; Delhalle, J.; Mekhalif, Z. Tantalum oxide/carbon nanotubes composite coatings on titanium, and their functionalization with organophosphonic molecular films: A high quality scaffold for hydroxyapatite growth. *J. Colloid Interface Sci.* **2012**, *371*, 150–158. [[CrossRef](#)] [[PubMed](#)]
42. Zhu, X.; Eibl, O.; Scheideler, L.; Geis-Gerstorf, J. Characterization of nano hydroxyapatite/collagen surfaces and cellular behaviors. *J. Biomed. Mater. Res. A* **2006**, *79*, 114–127. [[CrossRef](#)] [[PubMed](#)]
43. Lawrence, Y. *Anodic Oxide Films*; Academic Press: London, UK, 1961.

44. Kim, K.; Lee, B.-A.; Piao, X.-H.; Chung, H.-J.; Kim, Y.-J. Surface characteristics and bioactivity of an anodized titanium surface. *J. Periodontal Implant Sci.* **2013**, *43*, 198–205. [[CrossRef](#)] [[PubMed](#)]
45. Oh, H.-J.; Lee, J.-H.; Jeong, Y.; Kim, Y.-J.; Chi, C.-S. Microstructural characterization of biomedical titanium oxide film fabricated by electrochemical method. *Surf. Coat. Technol.* **2005**, *198*, 247–252. [[CrossRef](#)]
46. Yao, C.; Webster, T.J. Anodization: A promising nano-modification technique of titanium implants for orthopedic applications. *J. Nanosci. Nanotechnol.* **2006**, *6*, 2682–2692. [[CrossRef](#)] [[PubMed](#)]
47. Balasundaram, G.; Yao, C.; Webster, T.J. TiO<sub>2</sub> nanotubes functionalized with regions of bone morphogenetic protein-2 increases osteoblast adhesion. *J. Biomed. Mater. Res. A* **2008**, *84*, 447–453. [[CrossRef](#)] [[PubMed](#)]
48. Yamada, M.; Ueno, T.; Minamikawa, H.; Ikeda, T.; Nakagawa, K.; Ogawa, T. Early-stage osseointegration capability of a submicrofeatured titanium surface created by microroughening and anodic oxidation. *Clin. Oral Implant. Res.* **2013**, *24*, 991–1001. [[CrossRef](#)] [[PubMed](#)]
49. El-Wassefy, N.A.; Hammouda, I.M.; Habib, A.N.; El-Awady, G.Y.; Marzook, H.A. Assessment of anodized titanium implants bioactivity. *Clin. Oral Implant. Res.* **2014**, *25*, e1–e9. [[CrossRef](#)] [[PubMed](#)]
50. Le Guehennec, L.; Soueidan, A.; Layrolle, P.; Amouriq, Y. Surface treatments of titanium dental implants for rapid osseointegration. *Dent. Mater.* **2007**, *23*, 844–854. [[CrossRef](#)] [[PubMed](#)]
51. Wenzel, R.N. Resistance of solid surfaces to wetting by water. *Ind. Eng. Chem.* **1936**, *28*, 988–994. [[CrossRef](#)]
52. Herminghaus, S. Roughness-induced non-wetting. *EPL* **2000**, *52*, 165. [[CrossRef](#)]
53. Marmur, A. From hydrophilic to superhydrophobic: Theoretical conditions for making high-contact-angle surfaces from low-contact-angle materials. *Langmuir* **2008**, *24*, 7573–7579. [[CrossRef](#)] [[PubMed](#)]
54. Schwarz, F.; Wieland, M.; Schwartz, Z.; Zhao, G.; Rupp, F.; Geis-Gerstorfer, J.; Schedle, A.; Broggini, N.; Bornstein, M.M.; Buser, D.; et al. Potential of chemically modified hydrophilic surface characteristics to support tissue integration of titanium dental implants. *J. Biomed. Mater. Res. B Appl. Biomater.* **2009**, *88*, 544–557. [[CrossRef](#)] [[PubMed](#)]
55. Wennerberg, A.; Galli, S.; Albrektsson, T. Current knowledge about the hydrophilic and nanostructured SLActive surface. *Clin. Cosmet. Investig. Dent.* **2011**, *3*, 59–67. [[CrossRef](#)] [[PubMed](#)]
56. Sista, S.; Nouri, A.; Li, Y.; Wen, C.; Hodgson, P.D.; Pande, G. Cell biological responses of osteoblasts on anodized nanotubular surface of a titanium-zirconium alloy. *J. Biomed. Mater. Res. A* **2013**, *101*, 3416–3430. [[CrossRef](#)] [[PubMed](#)]



© 2018 by the authors. Licensee MDPI, Basel, Switzerland. This article is an open access article distributed under the terms and conditions of the Creative Commons Attribution (CC BY) license (<http://creativecommons.org/licenses/by/4.0/>).